Nanoscale

Accepted Manuscript

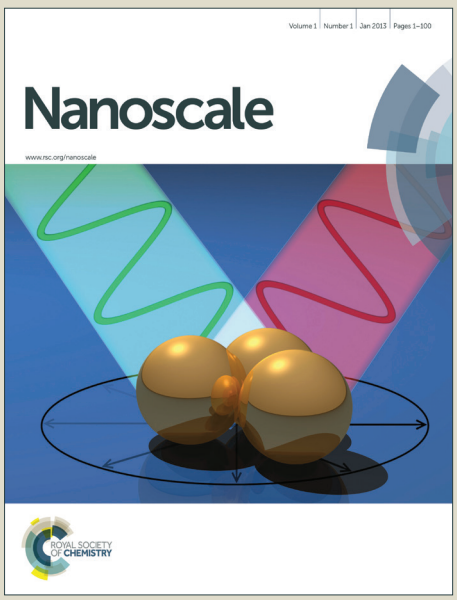

ROYAL SOCIETY OF CHEMISTRY

www.rsc.org/nanoscale

Cite this: DOI: 10.1039/c0xx00000x

www.rsc.org/xxxxxx

ARTICLE TYPE

Freestanding nanocellulose-composite fibre reinforced 3D polypyrrole electrodes for energy storage applications

Zhaohui Wang,*[a] Petter Tammela,[b] Peng Zhang,[b] Jinxing Huo,[c] Fredric Ericson,[d] Maria Strømme,*[b] Leif Nyholm*[a]

Received (in XXX, XXX) Xth XXXXXXXXX 20XX, Accepted Xth XXXXXXXXX 20XX
DOI: 10.1039/b000000x

It is demonstrated that 3D nanostructured polypyrrole (3D PPy) nanocomposites can be reinforced with PPy covered nanocellulose (PPy@nanocellulose) fibres to yield freestanding, mechanically strong and porosity optimised electrodes with large surface areas. Such PPy@nanocellulose reinforced 3D PPy materials can be employed as free-standing paper-like electrodes in symmetric energy storage devices exhibiting cell capacitances of 46 F g^{-1}, corresponding to specific electrode capacitances of up to ~185 F g^{-1} based on the weight of the electrode, and 5.5 F cm^{-2} at a current density of 2 mA cm^{-2}. After 3000 charge/discharge cycles at 30 mA cm^{-2}, the reinforced 3D PPy electrode material also showed a cell capacitance corresponding to 92 % of that initially obtained. The present findings open up new possibilities for the fabrication of high performance, low-cost and environmentally friendly energy-storage devices based on nanostructured paper-like materials.

Introduction

Electronically conducting polymers (ECPs), such as polypyrrole (PPy) and polyaniline (PANI) have recently attracted great attention for energy storage due to their high capacitance/capacity, low-cost, environment friendliness, ease of synthesis and flexibility in processing.[1-4] Their electrochemical performance has, however, been hampered by mass transport limitations for thick polymer layers and/or the mechanical stress resulting from repeated ion exchange.[3] As a result of this there have been many attempts to employ nanostructured ECPs[5-13] and ECP/carbon composites[14-19] and nanostructured three-dimensional (3D) ECP hydrogels or foams have shown promise for applications involving bioelectronics and electrochemical devices. The latter is mainly due to the high surface area, short diffusion paths and the continuous 3D conducting framework associated with these materials.[6, 7] Recently, it has been shown that 3D PANI hydrogels can exhibit specific capacitances of up to 480 F g^{-1} at a current density of 0.2 A g^{-1},[5] and that 3D PPy or PANI frameworks can be successfully utilised in high-performance Li-ion batteries.[20, 21] It should, however, be pointed out that most 3D ECP networks suggested for use in energy storage devices have relied on the use of substrates as a means of obtaining satisfactory mechanical properties. As the latter requires the inclusion of additional processing steps and also limits the possibilities to attain high active mass loadings, the use of substrates clearly makes the development of materials for low-cost and high energy density applications less straightforward.[22, 23]

Cellulose is the most abundant natural biopolymer, an almost inexhaustible raw material (extracted from wood, hemp, bacteria, algae, etc.) and a key source of sustainable materials which has found use in numerous applications outside the traditional ones linked to printing, packaging and cleaning.[24-31] Large-scale and energy-efficient production of nanocellulose fibres has recently been shown to yield promising improvements regarding the mechanical properties and the thermal stability of various host matrices.[3, 32] As cellulose is built up by repeating cellobiose units, containing six free hydroxyl groups, one acetal linkage and one hemiacetal linkage, there are strong inter- and intramolecular hydrogen bonds, providing fibres with high aspect ratios, hydroxyl functionalised surfaces and great axial elastic modulus. These combined properties make nanocellulose fibres a perfect building block in conjunction with other functional materials such as carbon nanotubes,[33, 34] PPy,[23, 35-37] graphene[38, 39] and PANI.[40, 41] Furthermore, when employed in electrochemical devices, cellulose fibres have also been suggested to provide pathways for ion transport.[42] Based on the issues above, it is reasonable to assume that nanocellulose functionalised with an ECP layer could be utilised to reinforce and support 3D ECP networks to create strong and flexible electrodes with properties that can be optimised both with respect to their mechanical integrity and electrochemical performance. Despite the fact that ECPs coated nanocellulose have shown a great potential for applications in battery and supercapacitors,[35, 37, 43-45] 3D

matrix-like, hybrid materials created thereof have not yet been utilised in energy storage devices.

Herein, we describe a facile *in situ* polymerisation process yielding PPy@nanocellulose reinforced 3D PPy composites. It is shown that only a small amount (i.e. 7 ~ 12 wt.%) of nanocellulose fibres is required to obtain a large surface area and to enhance the mechanical properties of the 3D PPy hydrogels significantly. The inclusion of the PPy@nanocellulose also gives rise to additional conductive paths through the material which should facilitate the charge transport. As is demonstrated PPy@nanocellulose reinforced 3D PPy with a mass loading of up to 30 mg cm^{-2}, can be directly used as freestanding electrodes in symmetric energy storage cells, exhibiting specific capacitances of up to 185 F g^{-1} (based on the weight of the electrode) and 5.5 F cm^{-2}, respectively, at a current density of 2 mA cm^{-2}. The present findings provide a new direction for the fabrication of low-cost and sustainable nanostructured materials for high-performance, paper-based energy-storage devices.

Experimental Section

Materials Synthesis

Cladophora green algae were collected from the Baltic Sea and the nanocellulose was extracted using grinding and acid hydrolysis as previously described.[46] Ammonium persulfate (APS), phytic acid and pyrrole (Py) were purchased from Sigma-Aldrich and used as received. Deionised water was used throughout the synthesis.

Preparation of 3D PPy nanocomposites: The 3D PPy samples (denoted 3D PPy) were synthesised according to a previously published protocol after slight modification.[5] Typically, 1.15 mL Py monomer and 3 mL phytic acid solution were added into 50 mL of DI water and magnetically stirred for 10 min at 0-5 °C. A solution containing 3.3 g APS, an oxidant initiating the polymerisation, in 20 mL of cold water was added to the above mixture under thorough stirring for one minute, after which the solution was kept still for 9 min to produce the 3D structured PPy. The 3D PPy was collected in a Büchner funnel connected to a suction flask, washed with DI water, and subsequently dried to yield a sheet. For comparison, granular PPy was prepared under the same condition but without assistance of phytic acid.

Preparation of PPy@nanocellulose reinforced 3D PPy: The *in situ* polymerisation of PPy@nanocellulose reinforced 3D PPy samples was performed as follows. First, 50 mg (or 100 mg) of *Cladophora* cellulose was dispersed in 50 mL water by sonication for a total pulse time of 10 min in the presence of water cooling. The sonication was carried out using a high-energy ultrasonic equipment (Sonics and Materials Inc., USA, Vibra-Cell 750) at an amplitude of 30% with a pulse length of 30 s and pulse-off duration of 30 s. A 50 ml solution containing Py (1.15 mL) and phytic acid (3 mL) was mixed with the cellulose dispersion and stirred for 10 min. The obtained composite was dried, washed and collected, in a similar manner as described for the synthesis of 3D PPy hydrogels. The weight of the cellulose and PPy in the composite was determined based on the weight of cellulose used in the preparation and the total weight of the product after drying. In this study the weight of the obtained 3D PPy-based material was 800 ± 40 mg. The PPy concentration in the composites containing 100 mg, 50 mg and 0 mg of nanocellulose, from here on denoted 3D PPy-2, 3D PPy-1 and 3D PPy, respectively, were estimated to be 88 %, 93 % and 100%, respectively.

Material and Electrochemical Characterisations

Scanning Electron Microscopy (SEM): SEM images for all samples were obtained employing a Leo Gemini 1550 FEG SEM instrument (Zeiss, Germany) operated at 8 kV employing an in-lens secondary electron detector. The samples were mounted on aluminium stubs with double-sided adhesive carbon tape and no sputtering was used prior to the imaging.

Transmission Electron Microscopy (TEM): Samples were prepared for TEM analysis by dispersing ground samples in ethanol in a sonication bath, after which a few drops of the dispersion were applied to the TEM sample holder and allowed to dry in air. Micrographs were recorded with a JEOL 2000 FXII microscope (JEOL, Tokyo, Japan) operated at 200 kV, with a LaB_6 filament.

Nitrogen sorption isotherm analysis: Nitrogen gas adsorption and desorption isotherms were obtained with an ASAP 2020 instrument (Micromeritics, USA). The specific surface area was calculated according to the Brunauer-Emmett-Teller (BET) method[47] employing the adsorption branch of the isotherm.

Bulk density and porosity: The bulk density, i.e., the ratio between the mass of the samples and the volume, was estimated from the dimensions of a piece of composite paper, using a high precision digital calliper (Mitutoyo, Japan). The bulk density of the 3D PPy-2, 3D PPy-1 and 3D PPy were 0.37, 0.38 and 0.41 g cm^{-3}, respectively. The porosity of all samples was estimated as $\varepsilon_{\%} = (1 - \rho_b/\rho_t) \times 100$, where $\varepsilon_{\%}$ is the porosity, ρ_b is the bulk density, ρ_t refers to true density. The porosities of the 3D PPy-2, 3D PPy-1 and 3D PPy were 77.4, 76.7 and 75.2%, respectively.

Mechanical tests: All three sample types under study (i.e. the 3D PPy, 3D PPy-1, and 3D PPy-2 samples) were characterised mechanically by measuring the Young's moduli using compression tests employing a Shimadzu Autograph AGS-X tensile machine and a 10 kN load cell. The compression tests were performed on square shaped samples (1 cm^{-2}) and the crosshead speed was 0.1 mm min^{-1}, corresponding to a strain rate of 0.1 min^{-1}. Two compression tests were performed for each of the sample types.

Cyclic voltammetry (CV): The CV measurements were performed at room temperature employing an Autolab/GPES instrument (ECO Chemie, The Netherlands) with the synthesised PPy-based electrodes as the working electrode in a three-electrode electrochemical cell also containing a platinum wire counter electrode and an Ag/AgCl reference electrode. The PPy-based electrodes used as the working electrode were cut into pieces weighing 4~6 mg. A platinum wire coiled around the PPy-based samples was used as the contact to these samples. An aqueous 2 M NaCl solution, which was purged with nitrogen for 15 min prior to the measurements, was used as the electrolyte. In the charge capacity calculations all values were normalised with respect to the total mass of the PPy-based electrode.

Assembly of symmetric energy storage devices: In the assembly of the symmetric devices a piece of ordinary filter paper was used as a separator between two rectangular pieces of the

composite PPy-based electrode (1 cm^2, weighing ~30 mg each). Graphite foils were used as current collectors while an aqueous 2 M NaCl solution was employed as the electrolyte. Prior to the assembly the electrolyte was purged with nitrogen for 15 min, after which the active material and the separator were wetted with the electrolyte. Cells were assembled and sealed in plastic coated aluminium foils.

Galvanostatic charge/discharge experiments and cycling stability measurements using symmetric devices: The rate capabilities of the different symmetric devices were investigated using galvanostatic charge/discharge experiments (employing the same equipment as used in the CV measurements) by applying current densities between 1 and 100 mA cm^{-2} (i.e. 0.033 to 3.3 A g^{-1} based on the weight of one electrode) within a cell voltage window ranging from 0 to 0.8 V. The cycling stability of the symmetric devices was evaluated from the results of galvanostatic charge/discharge experiments performed with a current density of 30 mA cm^{-2} (i.e. 1 A g^{-1}) within a cell voltage window ranging from 0 to 0.8 V. In all measurements the cells were compressed with a clip applying a force of about 25 N to ensure a good contact between the graphite foil current collector and the PPy-based electrodes.

The cell capacitances C of the symmetric devices were calculated from the galvanostatic discharge curves as $C = i\Delta t/\Delta V$, where i denotes the discharge current and ΔV the cell voltage change during the discharge time Δt. The gravimetric cell capacitances were calculated as $C_m=C/M$, where M refers to the total mass of the two PPy-based electrodes. The area-normalised cell capacitances were estimated as $C_a=C/S$, where S represents the cross-sectional area of the electrodes. The volumetric capacitances for single electrodes were estimated as $C_v=4\rho_b C_m$.

Electrochemical impedance spectroscopy studies of symmetric devices: The electrochemical impedance spectroscopy (EIS) measurements were performed with a CH Instruments 660D potentiostat (CH Instruments, Inc., USA) at a cell voltage of 0 V, using an ac amplitude of 10 mV and the frequency was varied between 100 kHz and 0.01 Hz. To ensure a good contact between the graphite foil current collector and the PPy-based electrodes a force equivalent to about 25 N was used also in these measurements.

Results and Discussion

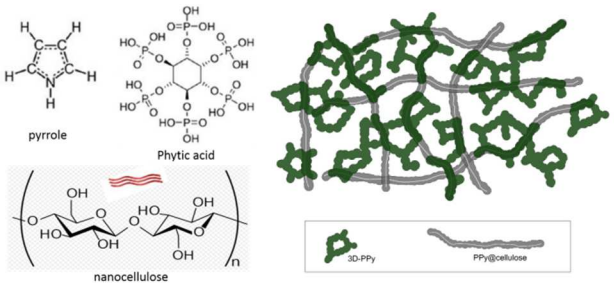

Fig. 1. Schematic illustration of the synthesis of the PPy@nanocellulose reinforced 3D PPy electrodes.

A schematic illustration of the synthesis of the PPy@nanocellulose-3D PPy composites is shown in Figure 1. The conductive and electroactive 3D network, which is obtained via the polymerisation of Py in the presence of phytic acid, contains both pores with a size of 20 to 50 nm (see Figure S1 in the Supporting information) facilitating the penetration of electrolyte ions, and micrometre-sized pores which help to accommodate the PPy volume changes during the redox processes.[3, 5] The inclusion of interweaved nanocellulose fibres (*in situ* coated with a thin (~50 nm) PPy layer) into the porous and conducting 3D network results in a 3D PPy material reinforced with nanocellulose fibres which has considerably improved mechanical properties compared to those for the pristine 3D PPy hydrogel. While the facile PPy coating onto the nanocellulose fibres can be explained by the facts that the cellulose fibres are well wetted by PPy and both cellulose and PPy have the ability to form hydrogen bonds via OH- and NH-groups, respectively, the phytic acid can serve as a counter ion for two separate PPy chains, thereby crosslinking them to yield a three-dimensional nanostructure. As a result, a porous and conducting PPy network reinforced with the nanocellulose fibres is readily obtained.

Cite this: DOI: 10.1039/c0xx00000x

www.rsc.org/xxxxxx

ARTICLE TYPE

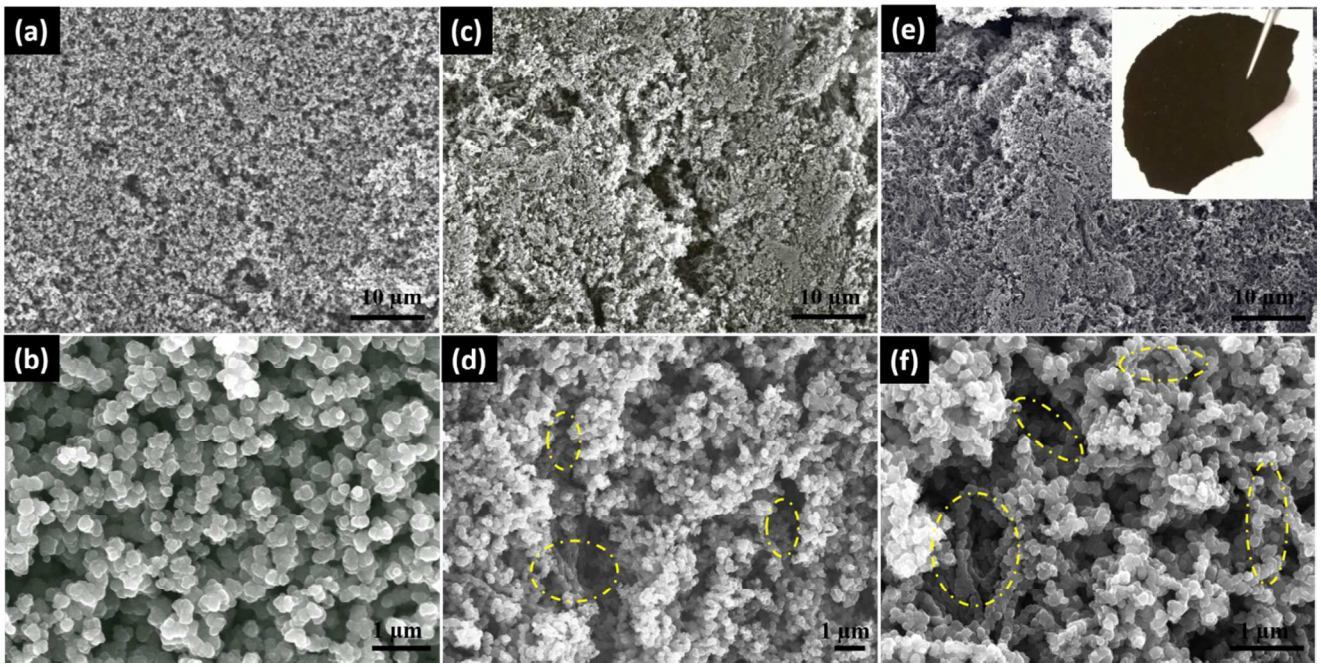

Fig. 2. SEM images for 3D PPy (a,b), 3D PPy -1 (c,d) and 3D PPy -2 (e,f). The dashed yellow ellipses indicate areas where the PPy@nanocellulose fibres can be seen. The inset in panel (e) shows a photograph of a 3D PPy -2 sample which has the appearance of a black paper sheet.

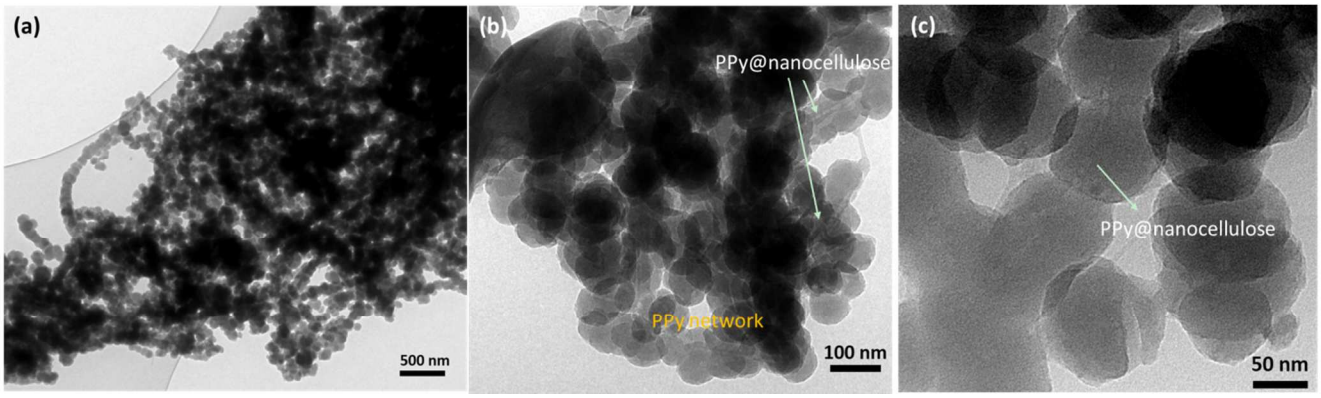

Fig. 3. TEM images for a 3D PPy-2 sample. The PPy@nanocellulose fibre entanglement in the 3D PPy network is depicted in (b) and the PPy coating on the nanocellulose fibres is seen in (c), which depict magnified images of the image (a).

Figure 2 shows SEM images of the 3D PPy hydrogel-based composite electrodes. Typically, the dried 3D PPy hydrogel consists of a hierarchical 3D porous foam-like network composed of dendritic nanospheres with typical diameters of ~ 100 nm (see Fig. 2a and b), forming a brittle but still free-standing material (see Fig. S2b in the Supporting Information). In contrast, when PPy is synthesised under identical conditions in absence of phytic acid, a powder consisting of agglomerated particles with diameters of 150-200 nm (see Fig. S2a in the Supporting Information) is formed. The latter demonstrates the shape- and structure-directing effect of phytic acid during the formation of the 3D conductive network. When a small amount (< 12 wt%, see the Experimental section) of nanocellulose is introduced during the preparation process, PPy spontaneously precipitates on the nanocellulose fibres forming a mechanically robust, and conductive backbone in intimate contact with the 3D conductive polymer hydrogel network. The SEM images of the composites (see Figure 2c-e), thus show a uniform mixture of PPy@nanocellulose fibres embedded in the highly porous 3D PPy matrix while the TEM images presented in Figure 3, display a ~50 nm PPy layer on the cellulose fibres in immediate contact with the PPy of the non-cellulose containing 3D PPy network.

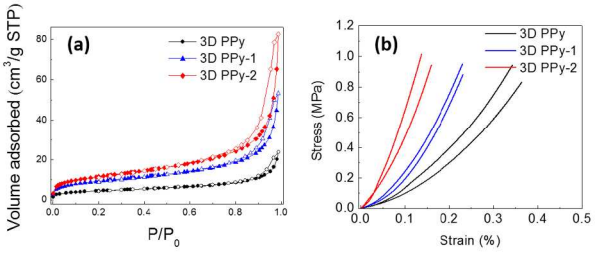

Fig. 4. Nitrogen adsorption/desorption isotherms (a) and stress-strain curves (b) from compression tests with the three types of 3D PPy composite electrodes under study.

The porous structures of the composites were further assessed by nitrogen-sorption isotherm analysis. Based on sorption isotherms of the type shown in Figure 4a, the BET surface area of the 3D PPy sample was found to be 16 m^2 g^{-1}. The PPy@nanocellulose reinforced 3D PPy composites exhibited larger surface areas, i.e. 32 and 39 m^2 g^{-1} for the 3D PPy-1 and 3D PPy-2 samples, respectively, indicating that only small amounts (i.e. 7 and 12 wt%) of nanocellulose significantly increase the nanostructure and hence the electrolyte accessible surface area of the material.

To study the mechanical properties of the 3D PPy composite samples under study, two compression tests were made for each sample type. The results, in terms of force-deflection data, were transformed into stresses and strains to enable the calculation of the elastic modulus for each composite. As can be seen from Figure 4b, a concave shaped arc was observed in the initial portion of all stress-strain curves. This is due to the fact that the contact between the compression plate of the test machine and the upper surface of the sample increased with increasing compression. To obtain the elastic modulus a linear curve fit was made to the linear part of the stress-strain curve (see in Table S1 in the Supporting Information). From this analysis the PPy@nanocellulose reinforced 3D PPy composites were found to exhibit ~2-4 times higher elastic moduli than the non-cellulose containing 3D PPy sample, indicating that the inclusion of the nanocellulose gives rise to significant improvements in the mechanical properties of the 3D PPy material.

To evaluate the effect of the incorporated nanocellulose on the electrochemical performance of the 3D PPy composites, CV experiments were performed at a number of scan rates between 5 and 200 mV s^{-1} (see Figure 5a-c). As is seen in Figure 5a, all samples displayed voltammograms with evident faradaic oxidation and reduction peaks at a scan rate of 5 mV s^{-1}. In these experiments, the potential window was adjusted for each scan rate so as to avoid PPy overoxidation by reversing the anodic potential scan before the overoxidation peak appeared. It can be seen that the oxidation peak appeared at more positive potentials for the non-cellulose containing 3D PPy sample than for the PPy@nanocellulose reinforced samples, indicating the presence of a larger iR drop and/or less facile electron-transfer kinetics[43] in the former case. The differences between the samples with and without nanocellulose became even more pronounced when the samples were cycled at higher scan rates (see Figure 5b and c). Even if no clear redox peaks could be observed for any of the samples at the highest scan rate (i.e. 200 mV s^{-1}, see Figure 5c), the PPy@nanocellulose reinforced 3D PPy samples still gave rise to larger currents than the non-cellulose containing 3D PPy sample when normalised with respect to the total weight of the electrode. These results indicate that the incorporated nanocellulose plays an important role in enhancing the electrochemical performances of the 3D PPy composite samples.

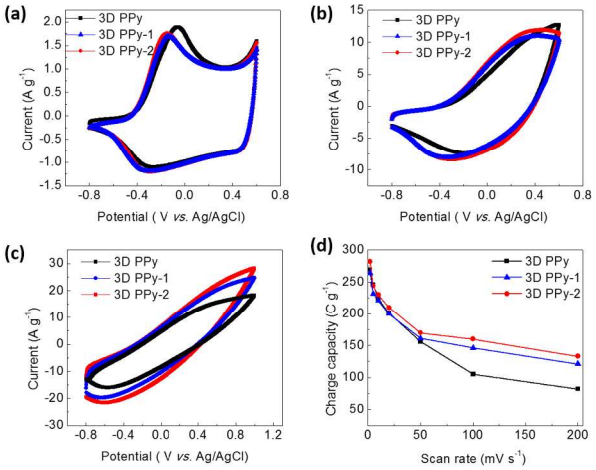

Fig. 5. Cyclic voltammograms recorded with a scan rate of 5 (a), 50 (b) and 200 (c) mV s^{-1} as well as the resulting charge capacities (d) for the 3D PPy composites under study. The currents and charge capacities were normalised with respect to the weight of the electrodes.

The charge capacities of the PPy-based electrodes were evaluated from the CV data and normalised with respect to the weight of the electrodes (see Figure 5d). No significant difference in the specific charge capacity could be observed for the samples at low scan rates as the values are all in the range between 264 and 282 C g^{-1}, translating into a specific capacity of ~ 75 mAh g^{-1}. The latter is slightly lower than previously published values (315 C g^{-1} and 88 mAh g^{-1}) for PPy@nanocellulose electrodes.[43] Although the charge capacities for all samples decreased with increasing scan rate, the PPy@nanocellulose reinforced 3D PPy samples clearly exhibited higher specific capacitances than the non-cellulose containing 3D PPy sample for scan rates above 20 mV s^{-1}. This finding, which is remarkable considering the fact that the normalisation was done with respect to the total weight of the electrode (i.e. including the weight of the non-electroactive cellulose, see Figure S3), indicates that the structure of the PPy@nanocellulose reinforced 3D PPy samples was more beneficial with respect to the mass transport within the electrodes. As the BET values were higher for these materials than for the non-cellulose containing 3D PPy sample it is reasonable to assume that this effect is linked to the slightly larger porosity and the larger surface area accessible to the electrolyte**.** As is seen in Figure S1 in the Supporting Information the volume of the mesopores increased with increasing amount of nanocellulose in the composites. The value of 133 C g^{-1} obtained for the 3D PPy-2 sample at a scan rate of 200 mV s^{-1} is incidentally comparable to the results previously reported for PPy-based paper electrodes.[43, 48, 49]

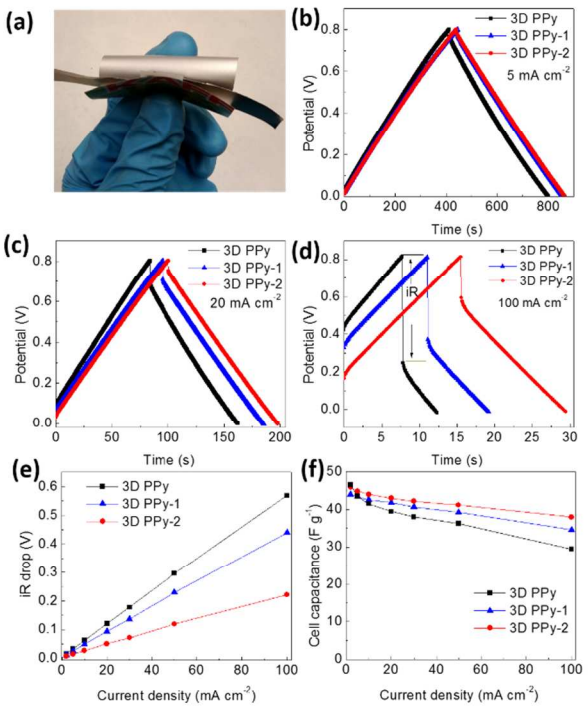

Fig. 6. Photograph showing the assembly of a 3D PPy-based cell with graphite foil current collectors (a). Galvanostatic charge/discharge curves for the composite electrodes obtained using 5 (b), 20 (c) and 100 (d) mA cm^{-2}. The evaluation of the iR drops is visualised in panel (d). Plots of the iR-drop (e) and cell capacitance (f) versus the current density. The cell capacitances were normalised with respect to the weight of both electrodes.

To further examine the electrochemical performance of the PPy@nanocellulose reinforced 3D PPy samples, symmetric energy storage devices were assembled as depicted in Figure 6a. The latter shows a photograph of a device containing two 3D PPy composite electrodes, graphite foil current collectors as well as a cellulose separator soaked with 2 M NaCl. As all component of the device are inexpensive, environmentally friendly and can be safely disposed of or incinerated after use,[3, 50] this kind of devices should have a significant potential for applications with a sustainablitiy focus.

Figures 6b, c and d show galvanostatic charge/discharge curves for the different symmetric devices using current densities of 5 mA cm^{-2}, 20 mA cm^{-2} and 100 mA cm^{-2}, respectively. The obtained linear charge and discharge curves are in excellent agreement with previously obtained results for PPy-based paper electrodes.[43, 48, 49] As is seen in Figure 6d and e, the influence of the iR drop was significantly smaller for the devices containing the PPy@nanocellulose reinforced 3D PPy electrodes indicating that the cell resistance of the latter devices was significantly lower. The cell resistances calculated from a linear fit to the data presented in Fig. 6e, were thus found to be 2.8, 2.2, and 1.1 Ω for the 3D PPy, 3D PPy-1 and 3D PPy-2 containing cells, respectively. Since it has been shown that the electrolyte resistance is one of the major contributions to the cell resistance,[51] this effect can most likely be ascribed to changes in the structure of the materials yielding a decreased electrolyte resistance within the pores of the material.

As is shown in Figure 6f and Figure S4 in the Supporting Information, the specific capacitances of the devices based on the PPy@nanocellulose reinforced 3D PPy electrodes were less affected by an increase in the charge/discharge current density than that containing non-cellulose containing 3D PPy electrodes. Whereas the latter device exhibited a cell capacitance of about 29 F g^{-1} at 100 mA cm^{-2}, the 3D PPy-2 electrode device gave rise to a cell capacitance of ~38 F g^{-1}, which was slightly higher than that for the 3D PPy-1 device (i.e. ~35 F g^{-1}). At the lowest current density, i.e. 2 mA cm^{-2}, all devices showed a cell capacitance of around 46 F g^{-1} (corresponding to a specific electrode capacitance of ~185 F g^{-1} or a volumetric electrode capacitance of ~72 F cm^{-3}), which is higher than the 40 F g^{-1} obtained for a device containing chopped carbon fibre (CCF) reinforced PPy-nanocellulose electrodes.[43] For the for 3D PPy-2 device this value corresponds to an area specific capacitance of 5.5 F cm^{-2}, which is noticeably higher than the values (< 2 F cm^{-2} in most cases) previously reported for nanostructured PANI-based electrodes.[36, 40, 43, 52, 53] The latter clearly illustrates the advantage of the unique structure obtained by reinforcing the 3D ECP network with PPy coated nanocellulose fibres.

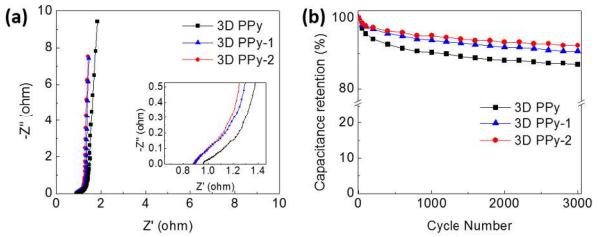

Fig. 7. Nyquist plots (a) and cycling stability performance (b) of symmetric cells comprising the different electrodes under study. The cycling experiments were conducted as galvanostatic charge/discharge experiments at 30 mA cm^{-2} for 3000 cycles and the capacitance values have been normalised with respect to the first cycle values.

As is seen in Figure 7a, the symmetrical devices were also studied using ac impedance spectroscopy. In analogy with the iR drop results, the high frequency resistance (obtained from the intercept between the Nyquist plot and the horizontal axis) was smaller for the device comprising PPy@nanocellulose reinforced 3D PPy electrodes supporting the hypothesis that the smaller resistance was due to a decreased electrolyte resistance within the pores of the electrodes. In contrast to the results of recent ac impedance measurements on symmetric devices containing PPy@nanocellulose electrodes,[54] no semicircles can be seen in the Nyquist plots in Figure 7a. This indicates that the ac impedance response became controlled by diffusion at higher frequencies (see the onset of the 45º slope in the Nyquist plots)[55]) than for the corresponding PPy@nanocellulose based devices. At even lower frequencies, a capacitive response due to finite length diffusion[55, 56] is seen for all three device types. The change from semi-infinite diffusion (45º slope) to finite length diffusion (capacitive, vertical line) occurred at similar frequencies, viz. at ~0.08-0.12 Hz, for all devices indicating that the diffusion coefficient for the Cl^- ions in the composites, as well as the time needed to reach the thin-layer conditions, were practically unaffected by the addition of PPy@nanocellulose fibres to the 3D PPy nanocomposite.

To evaluate the cycling stability of the 3D PPy based

symmetric devices, the cell capacitance was studied as a function of the cycle number using galvanostatic constant-current charge/discharge measurements conducted at 30 mA cm^{-2} in a cell voltage window between 0 and 0.8 V (see Figure 7b). As can be seen from the figure, the cell capacitance for the 3D PPy electrode based device decreased to 87% of its initial value over 3000 cycles. This represents a significantly higher stability than that previously reported for PPy-based supercapacitors (typically exhibiting 60 ~ 85% capacitance retention after 1000 cycles),[57, 58] and PPy nanowires (77 % capacitance retention after 700 cycles).[59] The good cycling performance achieved with the 3D PPy electrode-based cell clearly demonstrates the advantages associated with this highly porous interconnected nanostructure with respect to accommodating the swelling and shrinking of the polymer network during extended cycling.[7, 12] More importantly, however, the capacitance retention values for the PPy@nanocellulose reinforced 3D PPy electrode containing devices were even higher after 3000 cycles, viz. 91% and 92% for the 3D PPy-1 and the 3D PPy-2 containing cells, respectively. The latter values are incidentally also higher than previously reported values for carbon nanotube reinforced PPy nanowires[59] (exhibiting 85% capacitance retention after 1000 cycles) and uncoated cellulose nanofibre-supported ECP[60] (typically showing 75 ~ 90% capacitance retention after 1000 cycles). The improved cycling stability for cells containing the PPy@nanocellulose containing electrodes as compared to the non-cellulose containing ones was most likely due to the enhanced mechanical strength of the reinforced electrodes.[37, 45, 61] The latter is supported by the data presented in Table S1 in the Supporting Information. It should likewise be noted that the 3D PPy-2 composite electrodes still exhibited an area specific capacitance of 4.7 F cm^{-2} after 3000 charge/discharge cycles (see Figure S5 in the Supporting Information), a value which is considerably higher than those previously reported values for PPy@nanocellulose electrodes.[23, 43] This improvement can, at least partly, be explained by the fact that the 3D PPy-2 composites contained 88 % PPy and had a mass loading of 30 mg cm^{-2} while the corresponding values for pure PPy@nanocellulose electrodes typically were 65-70% and 10 ~ 20 mg cm^{-2}, respectively.

To summarise, the incorporation of PPy coated nanocellulose can clearly improve the electrochemical performance of 3D PPy composites significantly. As the nanocellulose does not contribute to the charge capacity of the composite materials, the obtained results can be interpreted as follows: the included PPy coated nanocellulose fibres serve as mechanical supports reinforcing the entire electrode as well as creating more pores and increased electrolyte contact area. This gives rise to a decreased cell resistance as hence *iR* drop which allows higher scan rates to be used without significant loss of charge capacity and much better cycling stability. The inclusion of *in situ* polymerised PPy@nanocellulose fibres into 3D PPy materials therefore constitutes a straightforward and inexpensive way of improving the electrochemical performance of conducting polymer-based hydrogel electrode materials. It should be pointed out that the cellulose-to-conducting polymer weight proportions used here only are of illustrative nature and that the mass loading of the composite therefore can be optimised further.

Conclusions

It is demonstrated that PPy@nanocellulose reinforced 3D PPy can be readily manufactured and employed as free-standing paper-like electrodes for efficient capacitive storage devices using a facile, low-cost, *in situ* polymerisation method. The introduction of PPy@nanocellulose fibres into the 3D PPy network leads to increased mechanical properties of the electrode material as well as to a larger surface area facilitating the contact between the electrolyte and the active material. Devices based on such electrodes are shown to exhibit higher charge capacities and capacitances at high scan rates when compared to devices based on non-cellulose containing 3D PPy materials. The PPy@nanocellulose reinforced 3D PPy devices also exhibit significantly higher cycling stabilities than their non-cellulose containing or carbon nanotube reinforced PPy counterparts as well as other similar cells based on other conducting polymers.

The present findings provide new possibilities to synthesise sustainable, low-cost and high performance energy-storage devices containing nanostructured materials.

Acknowledgements

The Swedish Foundation for Strategic Research (SSF) (grant RMA-110012), The Swedish Energy Agency (project SwedGrids), The Carl Trygger Foundation and the European Institute of Innovation and Technology under the KIC InnoEnergy NewMat and electrical energy storage project, are gratefully acknowledged for financial support of this work.

Notes and references

[a] *Department of Chemistry-The Ångström Laboratory, Uppsala University, Box 538, SE-751 21 Uppsala, Sweden, E-mail: zhaohui.wang@kemi.uu.se leif.nyholm@kemi.uu.se;*
[b] *Nanotechnology and Functional Materials, Department of Engineering Sciences, The Ångström Laboratory, Uppsala University, Box 534, SE-751 21 Uppsala, Sweden, E-mail: maria.stromme@angstrom.uu.se;*
[c] *Applied Mechanics, Department of Engineering Sciences, The Ångström Laboratory, Uppsala University, Box 534, SE-751 21 Uppsala, Sweden.*
[d] *Division of Microsystems Technology, Department of Engineering Sciences, The Ångström Laboratory, Uppsala University, Box 534, SE-751 21 Uppsala, Sweden.*

† Electronic Supplementary Information (ESI) available: [details of any supplementary information available should be included here]. See DOI: 10.1039/b000000x/

1. P. Novák, K. Müller, K. Santhanam and O. Haas, *Chem. Rev.*, 1997, **97**, 207-282.
2. G. Milczarek and O. Inganäs, *Science*, 2012, **335**, 1468-1471.
3. L. Nyholm, G. Nyström, A. Mihranyan and M. Strømme, *Adv. Mater.*, 2011, **23**, 3751-3769.
4. J. F. Mike and J. L. Lutkenhaus, *J. Poly. Sci. Part B: Poly. Phys.*, 2013, **51**, 468-480.
5. L. Pan, G. Yu, D. Zhai, H. R. Lee, W. Zhao, N. Liu, H. Wang, B. C. Tee, Y. Shi, Y. Cui and Z. Bao, *Proc. Natl. Acad. Sci. U. S. A.*, 2012, **109**, 9287-9292.
6. S. Ghosh and O. Inganäs, *Adv. Mater.*, 1999, **11**, 1214-1218.

7. Y. Zhao, B. R. Liu, L. J. Pan and G. Yu, *Energy Environ. Sci.*, 2013, **6**, 2856-2870.
8. D. O. Carlsson, G. Nyström, Q. Zhou, L. A. Berglund, L. Nyholm and M. Strømme, *J. Mater. Chem.*, 2012, **22**, 19014.
9. B. J.-W. Liu, J. Zheng, J.-L. Wang, J. Xu, H.-H. Li and S.-H. Yu, *Nano Lett.*, 2013.
10. Y. Zhao, J. Liu, Y. Hu, H. Cheng, C. Hu, C. Jiang, L. Jiang, A. Cao and L. Qu, *Adv. Mater.*, 2013, **25**, 591-595.
11. S. Y. Kim, J. Hong and G. T. R. Palmore, *Synth. Met.*, 2012, **162**, 1478-1481.
12. G. Yu, Y. Shi, P. Lijia, B. Liu, Y. Wang, Y. Cui and Z. Bao, *J. Mater. Chem. A*, 2014, **2**, 6086.
13. R. Temmer, R. Kiefer, A. Aabloo and T. Tamm, *J. Mater. Chem. A*, 2013, **1**, 15216-15219.
14. V. Gupta and N. Miura, *Electrochim. Acta*, 2006, **52**, 1721-1726.
15. S. R. Sivakkumar, W. J. Kim, J.-A. Choi, D. R. MacFarlane, M. Forsyth and D.-W. Kim, *J. Power Sources*, 2007, **171**, 1062-1068.
16. K. Jurewicz, S. Delpeux, V. Bertagna, F. Beguin and E. Frackowiak, *Chem. Phys. Lett.*, 2001, **347**, 36-40.
17. M. Hughes, G. Z. Chen, M. S. P. Shaffer, D. J. Fray and A. H. Windle, *Chem. Mater.*, 2002, **14**, 1610-1613.
18. P. Mini, A. Balakrishnan, S. V. Nair and K. Subramanian, *Chem. Commun.*, 2011, **47**, 5753-5755.
19. H.-H. Chang, C.-K. Chang, Y.-C. Tsai and C.-S. Liao, *Carbon*, 2012, **50**, 2331-2336.
20. H. Wu, G. Yu, L. Pan, N. Liu, M. T. McDowell, Z. Bao and Y. Cui, *Nat. Commun.*, 2013, **4**, 1943.
21. B. Liu, P. Soares, C. Checkles, Y. Zhao and G. Yu, *Nano Lett.*, 2013, **13**, 3414-3419.
22. Y. Gogotsi and P. Simon, *Science*, 2011, **334**, 917-918.
23. Z. Wang, P. Tammela, P. Zhang, M. Strømme and L. Nyholm, *J. Mater. Chem. A*, 2014, **2**, 7711-7716.
24. G. Zheng, Y. Cui, E. Karabulut, L. Wågberg, H. Zhu and L. Hu, *MRS Bull.*, 2013, **38**, 320-325.
25. D. Klemm, F. Kramer, S. Moritz, T. Lindström, M. Ankerfors, D. Gray and A. Dorris, *Angew. Chem. Int. Ed.*, 2011, **50**, 5438-5466.
26. Z. Shi, G. O. Phillips and G. Yang, *Nanoscale*, 2013, **5**, 3194-3201.
27. N. Ferraz, A. Leschinskaya, F. Toomadj, B. Fellström, M. Strømme and A. Mihranyan, *Cellulose*, 2013, **20**, 2959-2970.
28. G. Metreveli, L. Wågberg, E. Emmoth, S. Belák, M. Strømme and A. Mihranyan, *Adv. Health. Mater.*, 2014, DOI: 10.1002/adhm.201300641.
29. A. Mihranyan, *J. App. Poly. Sci.*, 2011, **119**, 2449-2460.
30. K. Hua, D. O. Carlsson, E. Alander, T. Lindström, M. Strømme, A. Mihranyan and N. Ferraz, *RSC Adv.*, 2014, **4**, 2892-2903.
31. K. Gelin, A. Bodin, P. Gatenholm, A. Mihranyan, K. Edwards and M. Strømme, *Polymer*, 2007, **48**, 7623-7631.
32. N. Lin, C. Bruzzese and A. Dufresne, *ACS Appl. Mater. Interfaces*, 2012, **4**, 4948-4959.
33. M. Wang, I. V. Anoshkin, A. G. Nasibulin, J. T. Korhonen, J. Seitsonen, J. Pere, E. I. Kauppinen, R. H. Ras and O. Ikkala, *Adv. Mater.*, 2013, **25**, 2428-2432.
34. L. Hu, J. W. Choi, Y. Yang, S. Jeong, F. La Mantia, L. F. Cui and Y. Cui, *Proc. Natl. Acad. Sci. U. S. A.*, 2009, **106**, 21490-21494.
35. G. Nyström, A. Mihranyan, A. Razaq, T. Lindström, L. Nyholm and M. Strømme, *J Phys. Chem. B*, 2010, **114**, 4178-4182.
36. L. Yuan, B. Yao, B. Hu, K. Huo, W. Chen and J. Zhou, *Energy Environ. Sci.*, 2013, **6**, 470-476.
37. G. Nyström, A. Razaq, M. Strømme, L. Nyholm and A. Mihranyan, *Nano Lett.*, 2009, **9**, 3635-3639.
38. Z. Weng, Y. Su, D.-W. Wang, F. Li, J. Du and H.-M. Cheng, *Adv. Energy Mater.*, 2011, **1**, 917-922.
39. J. M. Malho, P. Laaksonen, A. Walther, O. Ikkala and M. B. Linder, *Biomacromolecules*, 2012, **13**, 1093-1099.
40. B. Yao, L. Yuan, X. Xiao, J. Zhang, Y. Qi, J. Zhou, J. Zhou, B. Hu and W. Chen, *Nano Energy*, 2013, **2**, 1071-1078.
41. M. Pääkkö, J. Vapaavuori, R. Silvennoinen, H. Kosonen, M. Ankerfors, T. Lindström, L. A. Berglund and O. Ikkala, *Soft Matter.*, 2008, **4**, 2492-2499.
42. Z. Gui, H. Zhu, E. Gillette, X. Han, G. W. Rubloff, L. Hu and S. B. Lee, *ACS Nano*, 2013, **7**, 6037-6046.
43. A. Razaq, L. Nyholm, M. Sjödin, M. Strømme and A. Mihranyan, *Adv. Energy Mater.,* 2012, **2**, 445-454.
44. W. Hu, S. Chen, Z. Yang, L. Liu and H. Wang, *J Phys. Chem. B*, 2011, **115**, 8453-8457.
45. H. Olsson, D. O. Carlsson, G. Nyström, M. Sjödin, L. Nyholm and M. Strømme, *J. Mater. Sci.*, 2012, **47**, 5317-5325.
46. A. Mihranyan, A. P. Llagostera, R. Karmhag, M. Strømme and R. Ek, *Inter. J. Pharma.*, 2004, **269**, 433-442.
47. S. Brunauer, P. H. Emmett and E. Teller, *J. Am. Chem. Soc.*, 1938, **60**, 309-319.
48. R. A. Davoglio, S. R. Biaggio, N. Bocchi and R. C. Rocha-Filho, *Electrochim. Acta*, 2013, **93**, 93-100.
49. H. K. Song and G. T. R. Palmore, *Adv. Mater.*, 2006, **18**, 1764-1768.
50. B. Dyatkin, V. Presser, M. Heon, M. R. Lukatskaya, M. Beidaghi and Y. Gogotsi, *ChemSusChem*, 2013, **6**, 2269–2280.
51. G. Nyström, M. Strømme, M. Sjödin and L. Nyholm, *Electrochim. Acta*, 2012, **70**, 91-97.
52. Y.-Y. Horng, Y.-C. Lu, Y.-K. Hsu, C.-C. Chen, L.-C. Chen and K.-H. Chen, *J. Power Sources*, 2010, **195**, 4418-4422.
53. J. Wang, Y. Yang, Z.-H. Huang and F. Kang, *J. Mater. Chem.*, 2012, **22**, 16943-16949.
54. P. Tammela, H. Olsson, M. Strømme and L. Nyholm, *J Power Source*, 2014, submitted
55. C. Ho, I. Raistrick and R. Huggins, *J. Electrochem. Soc.*, 1980, **127**, 343-350.
56. M. Strømme Mattsson, G. Niklasson and C. Granqvist, *J. App. phys.*, 1996, **80**, 2169-2174.
57. Y. Yan, Q. Cheng, G. Wang and C. Li, *J. Power Sources*, 2011, **196**, 7835-7840.
58. Q. Liu, M. H. Nayfeh and S.-T. Yau, *J. Power Sources*, 2010, **195**, 3956-3959.
59. H. Fu, Z.-J. Du, W. Zou, H.-q. Li and C. Zhang, *J. Mater. Chem. A*, 2013, **1**, 14943-14950.
60. Y.-W. Ju, G.-R. Choi, H.-R. Jung and W.-J. Lee, *Electrochim. Acta*, 2008, **53**, 5796-5803.
61. A. Mihranyan, L. Nyholm, A. E. Garcia-Bennett and M. Strømme, *J. Phys. Chem. B*, 2008, **112**, 12249-12255.